PHYSICAL REVIEW B, VOLUME 64, 092401

Soft-x-ray small-angle scattering as a sensitive probe of magnetic and charge heterogeneity

J. B. Kortright,[1] Sang-Koog Kim,[1,*] G. P. Denbeaux,[1] G. Zeltzer,[2,†] K. Takano,[2] and Eric E. Fullerton[2]
[1]*Materials Science Division, Lawrence Berkeley National Laboratory, Berkeley, California 94720*
[2]*IBM Almaden Research Center, 650 Harry Road, San Jose, California 95120*

(Received 4 May 2001; published 25 July 2001)

Cobalt 2*p* resonant scattering from Co/Pt multilayers with perpendicular anisotropy results from magnetic and chemical heterogeneity having very different length scales. Magnetic and chemical scattering result from domains and the crystalline grain structure, respectively, as confirmed by field-dependent scattering and by imaging using magnetic x-ray and atomic force microscopy. Magnetic and charge scattering have distinct energy spectra that are quantitatively modeled using measured Co scattering factors. Domain and chemical correlations remain uncoupled throughout the reversal process.

DOI: 10.1103/PhysRevB.64.092401 PACS number(s): 75.60.−d, 75.25.+z, 75.70.Kw, 78.20.Ls

Fluctuations or heterogeneity in magnetization **M** are ubiquitous in temperature- and field-dependent phase transitions,[1] and are often associated with static or quasistatic magnetization distributions in the form of remnant domains and their walls. Length scales of interest for **M** heterogeneity range from interatomic exchange lengths to many microns, with exchange stiffness lengths in the 6–20 nm range determining common length scales over which **M** variation is expected in otherwise homogeneous material. Many techniques measure the average magnetization in volumes probed experimentally, but few can resolve its spatial distribution over 1–200 nm length scales. Neutron scattering has been the tool of choice to study magnetic structure and fluctuations even in thin films.[2,3,4] Emerging soft-x-ray resonant scattering techniques are also sensitive to structure in **M**.[5] Resonant specular and off-specular reflectivity measurements have demonstrated sensitivity to magnetic structure in films imposed by chemical heterogeneity in single[6] or multilayer[7,8] films or by roughness at interfaces[9,10] and to regular arrays of stripe domains.[11,12] Traditional small-angle scattering (SAS) at soft-x-ray core resonances has observed nanoscale chemical heterogeneity in alloy films.[13]

This report demonstrates that resonant soft-x-ray scattering from magnetic heterogeneity can be orders of magnitude stronger than resonant charge scattering in otherwise traditional SAS measurements. Magnetic and charge scattering are resolved through characteristic scattering vector, applied field, and spectral dependences. While microscopy techniques confirm these determinations of magnetic and charge sources of scattering for the samples studied, this complement of resonant scattering techniques yields information not readily obtainable from conventional microscopy or neutron scattering methods.

Co/Pt multilayers having perpendicular magnetic anisotropy provide ideal samples to study SAS from magnetic heterogeneity in the form of domains. The two samples described here were grown by magnetron sputtering in 3 mTorr Ar onto amorphous SiN_x (160 nm) membrane substrates to have nominal structure $\mathrm{Pt(20\,nm)/[Co(}t_{\mathrm{Co}})/\mathrm{Pt}(t_{\mathrm{Pt}})]_{50}\mathrm{Pt(3\,nm)}$. Sample *A* was grown at 250 °C with $t_{\mathrm{Co}} = 0.4$ nm and $t_{\mathrm{Pt}} = 0.7$ nm, while sample *B* was grown at ambient temperature with $t_{\mathrm{Co}} = 0.6$ nm and $t_{\mathrm{Pt}} = 0.4$ nm. These growth conditions yield relatively smooth multilayer films with perpendicular magnetic anisotropies exceeding the thin-film dipolar energies. These films exhibit little resistance to the nucleation of randomly oriented reverse domains. These domains, imaged at normal incidence using a transmission x-ray microscope[14] with Co magnetic circular dichroism contrast, are shown as the inset in Fig. 1(a) and form the magnetic fluctuations of interest here. Scattering measurements were made at the Advanced Light Source on linearly and elliptically polarizing undulator beamlines using linear polarization except as noted. The symmetric transmission

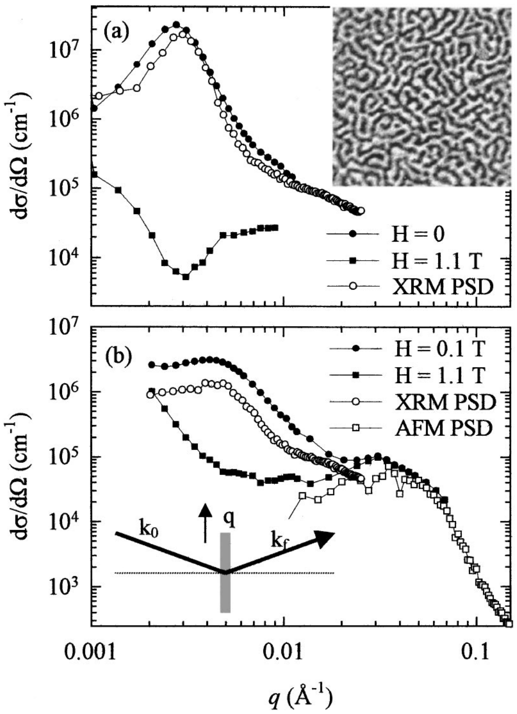

FIG. 1. (a) *q*-resolved SAS at remanance and saturation for sample *A*, with 4×4 micron image of remnant stripe domains (inset). The scaled PSD of the domain contrast is plotted. (b) similar SAS data for sample *B*, with PSDs from its domain image and from its AFM surface height image. The symmetric transmission geometry (inset) with scattering vector **q** defined by incident and scattered wave vectors $\mathbf{k_0}$ and $\mathbf{k_f}$. The longitudinal resolution is $\Delta q = 0.002$ Å^{-1}.

scattering geometry [Fig. 1(b), inset] was used to constrain the scattering vector $\mathbf{q}=\mathbf{k}_0-\mathbf{k}_f$ in the film plane to optimize coupling to the magnetic structure. This geometry also avoids a varying-depth sensitivity with q (Ref. 15) and distorted-wave effects associated with diffuse scattering near the specular beam and the critical angle for total reflection.[15,16]

Strong SAS is observed in q scans from each sample as seen in Fig. 1. Data were collected at the maximum in the Co L_3 resonance (see below), either in a saturating field ($\mathbf{H}=1.1\,\mathrm{T}$) normal to the sample surface or near remanance [$\mathbf{H}=0$, Fig. 1(a), and $\mathbf{H}=0.1\,\mathrm{T}$, Fig. 1(b)]. The data are normalized to the absolute differential scattering cross section $d\sigma(q)/d\Omega$ given by the scattered flux per solid angle per sample volume normalized by the incident flux. The q scans near remanance show a strong peak at $q=0.0027\,\text{Å}^{-1}$ for sample *A* and a somewhat weaker and broader peak at $q=0.0042\,\text{Å}^{-1}$ for sample *B*. The intensity in each peak is suppressed by orders of magnitude when the samples are saturated, clear evidence that they result primarily from magnetic scattering. The power spectral density (PSD) of the domains in Fig. 1(a), obtained from the image as the square of its Fourier transform, is scaled and plotted to confirm the magnetic origin of this peak for sample *A*. The PSD from a similar x-ray domain image also confirms the magnetic origin of the low-q peak for sample *B* in Fig. 1(b). The average spacing between domains is estimated from $2\pi/q_{\text{peak}}$ as 230 and 150 nm for samples *A* and *B*, respectively, with sample *A* exhibiting a narrower, more intense peak than sample *B*, consistent with a sharper domain size distribution. The resonant scattering cross sections at the magnetic peaks are many orders of magnitude larger than typically found in magnetic neutron SAS.[4]

The scattering at saturation shows two distinct features; each is predominantly chemical, not magnetic, in origin. For each sample the intensity first decreases and then increases with increasing q. The distinct peak for sample *B* at $q=0.031\,\text{Å}^{-1}$ corresponds to a 20-nm spacing. The PSD of its surface height as determined by atomic force microscopy (AFM) is scaled and plotted in Fig. 1(b). The AFM image shows features typical of a polycrystalline film, with the 20-nm spacing characterizing the height fluctuations of adjacent columnar grains. This peak thus originates the granular structure of the polycrystalline film. The increase in scattering to low q shows some differences between the two samples, but is also observed in uncoated SiN_x membranes, suggesting that this scattering originates from the substrates. The distinct differences in scattering for each sample near remanance and at saturation, and the differences between the samples, reveal that the SAS is sensitive both to chemical and magnetic structure within the films over length scales of 2–300 nm.

The Co atomic scattering factor $f_{\mathrm{Co}}(h\nu)$ describes magnetic and charge scattering. Including resonant charge and magnetic and nonresonant charge contributions,[17]

$$f=(\mathbf{e}_f^*\cdot\mathbf{e}_0)f_c+i(\mathbf{e}_f^*\times\mathbf{e}_0)\cdot\mathbf{m}f_{m1}+(\mathbf{e}_f^*\cdot\mathbf{m})(\mathbf{e}_0\cdot\mathbf{m})f_{m2},$$

where $\mathbf{e}_0$ and $\mathbf{e}_f$ are polarization vectors of incident and scattered x rays and $\mathbf{m}$ is a unit vector in the direction of the local magnetization. Three distinct polarization dependences accompany the complex charge (f_c), first-order magnetic (f_{m1}), and second-order magnetic (f_{m2}) amplitudes, each of which is defined in terms of different linear combinations of the spherical harmonics describing the $2p$ to $3d$ dipole transition matrix elements. The scattering observed here is in the near-forward (z) direction, and the domains have $\mathbf{m}$ also along z, maximizing sensitivity to f_{m1}. Since f_{m2} is generally small compared to f_{m1} (Ref. 15) and is further reduced by the geometry used, $f_\pm\cong f_c\pm f_{m1}$. Magnetic SAS using linear polarization, like Faraday and Kerr rotation, is understood in terms of these different scattering amplitudes for the opposite helicity circular components that form the linearly polarized beam. Interference between charge and magnetic amplitudes[18] has been of interest in specular and off-specular scattering from magnetic films.[19]

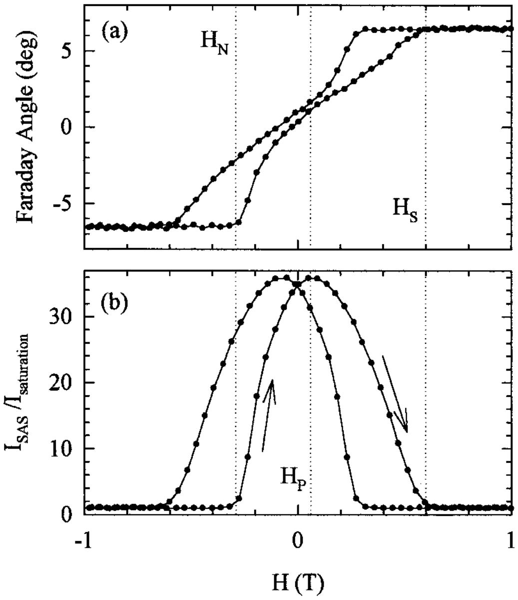

FIG. 2. (a) Faraday rotation hysteresis loop measures the *average* Co magnetization in the illuminated volume of sample B. (b) SAS hysteresis loop for $q=0.0042\,\text{Å}^{-1}$ measures *deviations from average* magnetization resulting from the domains that mediate the reversal. Vertical lines at $\mathbf{H}_N$, $\mathbf{H}_P$, and $\mathbf{H}_S$ are guides to the eye.

The field dependence of the SAS complements not only its q dependence, but also the average $\mathbf{M}(\mathbf{H})$ loop, as seen for sample *B* in Fig. 2. The average Co magnetization is displayed in Fig. 2(a) as a hysteresis loop measured by the Faraday rotation of x rays in transmission tuned just below the Co L_3 line. The shape of this loop is identical to that measured by polar magneto-optic Kerr effect in the visible. A negative nucleation field $\mathbf{H}_N$ and small remanance and coercive field $\mathbf{H}_C$ characterize $\mathbf{M}(\mathbf{H})$ normal to the sample, revealing little resistance to domain formation. The SAS loop measured at $q=0.0042\,\text{Å}^{-1}$ is shown in Fig. 2(b) and results from *deviations from the average* magnetization that occur during reversal. From negative saturation, scattering commences to increase at $\mathbf{H}_N$ by orders of magnitude to a maximum and falls back to the saturation level at $\mathbf{H}_S$. Here $\mathbf{H}_N$ and $\mathbf{H}_S$ coincide with the onset and saturation of reversal as measured in the Faraday rotation loop and signal the initial nucleation and final annihilation of the domains that mediate reversal[20] and whose scattering is directly measured. The shape of the SAS loop measures the amplitude variation of **M** during reversal at the in-plane frequency q. The maximum scattering occurs at the peak field $\mathbf{H}_P \simeq 0.1$ T, which is larger than $\mathbf{H}_C$ and does not correlate with any feature in the average $\mathbf{M}(\mathbf{H})$ loop. $\mathbf{H}_C$ is the field of zero net **M** along the film normal, while $\mathbf{H}_P$ is the field for maximum amplitude variation. The difference between $\mathbf{H}_P$ and $\mathbf{H}_C$ implies either that some fraction of **M** is oriented away from the film normal at $\mathbf{H}_C$ (and q) or that the average domain spacing depends on **H**, or both. However, measured SAS loops out to the chemical peak at $q = 0.031$ Å^{-1} show no significant change in $\mathbf{H}_P$ or the loop shapes. The former situation would arise from domain walls or closure domains having non-normal **M** components, suggesting that $\mathbf{H}_P$ is shifted from $\mathbf{H}_C$ towards the remnant coercivity where half of the sample has switched irreversibly. This frequency-dependent information on the evolution of magnetic disorder with field is difficult to obtain using other techniques and is clearly important in understanding reversal processes.

There is no doubt about the magnetic and charge origins of scattering for the samples studied here, largely because of their very different q and **H** dependences. In general, samples may not so readily yield this information, especially when the length scales of magnetic and charge heterogeneity are more equal. Thus it is important to have other means to determine whether measured scattering originates from magnetic-magnetic, charge-charge, or charge-magnetic interference. The spectral dependence of the scattering, in conjunction with modeling, provides a general means to analyze this problem.

Spectral scans for sample B at $q \cong 0.0042$ and 0.031 Å^{-1} are shown in Figs. 3(a) and 3(b), respectively. Each panel shows spectra at saturation and at $\mathbf{H}_P$. At $q \cong 0.0042$ Å^{-1} large peaks are observed at the Co L_3 and L_2 lines at $\mathbf{H}_P$ when domains are present and are entirely suppressed at saturation. At $q \cong 0.031$ Å^{-1} resonant features are observed at *both* saturation and $\mathbf{H}_P$. The resonant shapes are quite different at the high-q peak, each exhibiting bipolar character with that at $\mathbf{H}_P$ more intense near the L_3 and L_2 lines. The weaker overall resonant variation at the higher-q than the lower-q peak is consistent with scattering from elements other than Co at this charge peak. Knowledge of the Co scattering factors $f_\pm = f_c \pm f_{m1}$ is essential to model the spectra in Figs. 3(a) and 3(b). These were obtained from normal-incidence transmission absorption measurements using circular polarization and reversing the helicity or the direction of saturated **M**. The measured quantities are the imaginary parts of $f_+ = f_c + f_{m1}$ and $f_- = f_c - f_{m1}$, from which the real parts are obtained by Kramers-Kronig transformation to determine f_c and f_{m1} in Fig. 3(c).

Modeling SAS spectra proceeds by positing a specific scattering mechanism, calculating its spectrum, comparing with measurement, and iterating to self-consistency. Assuming multiple-scattering sources, the general amplitude is $A = \sum_i a_i s_i$, where the sum is over each source, a_i is its strength, and s_i describes its spatial distribution. Two sources, corresponding to the magnetic (a_m) and charge (a_c) scattering represented by the PSDs in Fig. 1(b), are assumed here, yielding intensity in the single-scattering approximation proportional to $A^*A = a_m^* a_m s_{m-m} + a_c^* a_c s_{c-c} + 2\,\mathrm{Re}[a_m^* a_c] s_{m-c}$. Here magnetic-magnetic, charge-charge, and magnetic-charge interference terms are explicit, the s_{i-j} contain all structural information, and $a_i^* a_j$ contain all f, $\mathbf{e}_{0,f}$, and **m** information. Only these latter terms are needed to calculate SAS spectra. Since pure circular components scatter only into the same helicity for both magnetic and charge amplitudes, the scattering from each helicity is calculated separately. Model spectra are multiplied by the measured transmission for comparison with measured spectra.

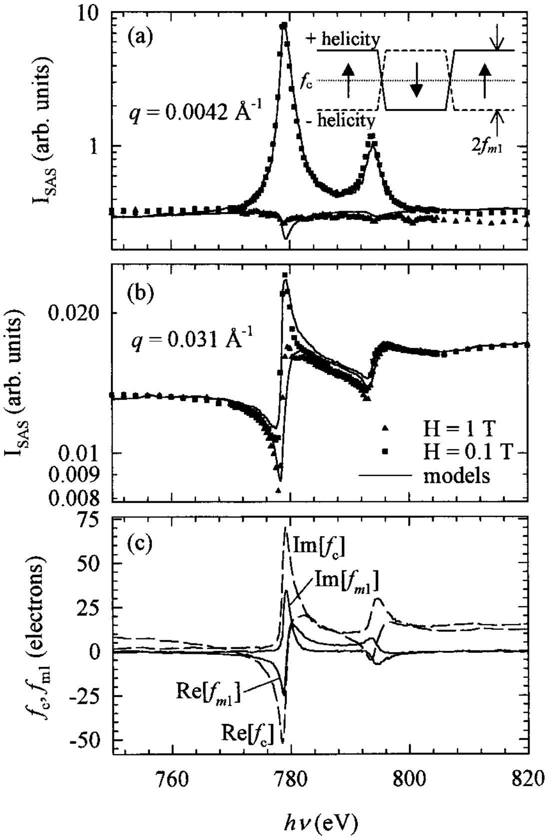

FIG. 3. Measured SAS spectra at saturation and 0.1 T measured at $q \cong 0.0042$ and 0.031 Å^{-1} are in (a) and (b), respectively. Real and imaginary parts of measured charge (f_c) and magnetic (f_{m1}) scattering factors are in (c) and are used to model the spectra in (a) and (b) as solid lines (see the text for details).

The pure magnetic amplitude for each helicity from oppositely magnetized domains is given by $a_m = f_+ - f_- = 2\,f_{m1}$ as shown schematically in Fig. 3(a) (inset). Only the difference in the magnetic part of f_{Co} contributes to this amplitude, since any Co and Pt charge scattering does not vary across domain boundaries. The intensity spectrum from pure magnetic scattering, proportional to $a_m^* a_m$, is scaled and plotted together with a pure charge background in Fig. 3(a) to show excellent agreement with the spectra measured at $\mathbf{H}_P$. The pure charge background (see below) is plotted alone and shows good agreement with the saturated scattering.

Many possibilities exist to model the charge amplitude. From AFM data a reasonable model assumes that surface roughness is the source of charge scattering and is modeled with scattering contrast given by the difference between some linear combination of Co and Pt scattering factors and vacuum. Iterative modeling leads to $a_c = f_{\mathrm{Co},c} + 3 f_{\mathrm{Pt}}$ for the charge amplitude that closely fits the saturated scattering at $q = 0.031$ Å^{-1} as in Fig. 3(b). This combination of Co and Pt scattering is reasonable, considering that the multilayer has a Pt cap layer. Tabulated values[21] are used for f_{Pt}, whose slowly varying but significant real and imaginary parts are key in obtaining the correct shape of the Co resonant features. Models using amplitude contrast between just Co and either vacuum or Pt were unable to fit the spectra. A pure magnetic contribution is added to this pure charge contribution (in 5:4 ratio) to model the high-q spectra measured at $\mathbf{H}_P = 0.1$ T in Fig. 3(b). The spectral shape of the cross term $\mathrm{Re}[a_m^* a_c]$ using these models for a_m and a_c is distinctly different from the pure magnetic and charge spectra, and does not agree with any of the measured spectra or improve the fit when added to these other contributions. This is not surprising given the well-separated PSD's of domains and roughness for this sample (the average domain size is 10 times the grain size). As seen in Fig. 3(c), only $a_m^* a_m$ exhibits strictly positive resonant features since $|f_{m1}|$ remains nonzero in the resonant region, while $|f_c|$ has sharp minima[15] that are related to the general bipolar character of a_c. These characteristic spectral shapes aid in making this modeling approach a valuable technique to determine the charge or magnetic origin of scattering. While *s*-to-*p* scattering is sometimes used to identify magnetic scattering, simply the propagation of incident or scattered radiation through magnetized regions produces just such a rotation of polarization. This spectral technique may thus provide the most reliable general means to resolve magnetic from charge scattering and identifying their sources.

In summary, these results reveal an impressive sensitivity of resonant soft-x-ray SAS to both magnetic and charge heterogeneity at length scales from 300 down to 10 nm, with straightforward extension down to roughly 1 nm in backscattering geometry. The strong resonant cross sections yield higher sensitivity for soft-x-ray compared to neutron SAS. The simultaneous sensitivity to magnetic and chemical heterogeneity through both field and spectral variation, together with spatial sensitivity down to the nm scale, provides information unattainable through conventional microscopy techniques. These techniques consistently show that magnetization and grain correlation lengths remain uncoupled throughout reversal in the samples studied. Continued application of these techniques will provide new information about the magnetic structure and reversal in films with perpendicular anisotropy and about nanoscale magnetic and chemical structure and phase transitions in a broad range of samples.

Work at LBNL was supported by the Director, Office of Energy Research, Office of Basic Energy Sciences, Materials Sciences Division, of the U.S. Department of Energy under Contract No. DE-AC03-76SF00098.

---

[*] Current address: Department of Physics and CNSM, Korea Advanced Institute of Science and Technology, Teajon, 305-701, Korea.

[†] Current address: Department of Applied Physics, Stanford University, Stanford, CA 94305.

[1] M. F. Collins, *Magnetic Critical Scattering* (Oxford University Press, New York, 1989).

[2] J. A. Borchers *et al.*, Phys. Rev. Lett. **82**, 2796 (1999).

[3] J. F. Ankner and G. P. Felcher, J. Magn. Magn. Mater. **200**, 741 (1999).

[4] F. Hellman *et al.*, Phys. Rev. B **59**, 11 408 (1999).

[5] J. B. Kortright *et al.*, J. Magn. Magn. Mater. **207**, 7 (1999).

[6] C. C. Kao *et al.*, Phys. Rev. Lett. **65**, 373 (1990).

[7] J. M. Tonnerre *et al.*, Phys. Rev. Lett. **75**, 740 (1995).

[8] Y. U. Idzerda, V. Chakarian, and J. W. Freeland, Phys. Rev. Lett. **82**, 1562 (1999).

[9] J. F. MacKay *et al.*, Phys. Rev. Lett. **77**, 3925 (1996).

[10] J. W. Freeland *et al.*, Phys. Rev. B **60**, R9923 (1999).

[11] H. A. Dürr *et al.*, Science **284**, 2166 (1999).

[12] E. Dudzik *et al.*, Phys. Rev. B **62**, 5779 (2000).

[13] J. B. Kortright, S.-K. Kim, and H. Ohldag, Phys. Rev. B **61**, 64 (2000).

[14] The imaging x-ray microscope on ALS bending magnet beamline 6.1.2 was used to produce this image.

[15] J. B. Kortright and S.-K. Kim, Phys. Rev. B **62**, 12 216 (2000).

[16] S. K. Sinha *et al.*, Phys. Rev. B **38**, 2297 (1988).

[17] J. P. Hannon *et al.*, Phys. Rev. Lett. **61**, 1245 (1988); **62**, 2644(E) (1989).

[18] S. W. Lovesey and S. P. Collins, *X-Ray Scattering and Absorption by Magnetic Materials* (Oxford University Press, New York, 1996).

[19] R. M. Osgood III *et al.*, J. Magn. Magn. Mater. **198**, 698 (1999).

[20] C. Kooy and U. Enz, Philips Res. Rep. **15**, 7 (1960).

[21] B. L. Henke, E. M. Gullikson, and J. C. Davis, At. Data Nucl. Data Tables **54**, 181 (1993), and at http://www-cxro.lbl.gov/optical_constants/